A Wearable Graphene Transistor-Based Biosensor for Monitoring IL-6 Biomarker

- Kaitlyn E. Laliberte¹, Patrick Scott¹, Niazul I. Khan¹, MD Shaad Mahmud¹, Edward Song^{1,2*} 1
- ¹Department of Electrical and Computer Engineering, University of New Hampshire, Durham, NH, 2
- USA 3
- 4 ²Materials Science Program, University of New Hampshire, Durham, NH, USA
- 5 * Correspondence:
- 6 **Edward Song**
- Edward.Song@unh.edu 7
- 8 Keywords: graphene, field-effect transistor, printable, wearable, biosensor, aptamer,
- interleukin-6 9
- 10 **Abstract**
- Graphene-based field-effect transistor (GFET) is becoming an increasingly popular biosensing 11
- platform for monitoring health conditions through biomarker detection. Moreover, the graphene's 2-12
- dimensional geometry makes it ideal for implementing flexible or wearable electronic devices. If 13
- implemented as a wearable biosensor, such technology can non-invasively monitor relevant 14
- biomarkers continuously in real-time and alert the user of possible health concerns. As a proof of 15
- feasibility, this paper presents a wearable GFET device fabricated on a flexible film that is capable of 16
- detecting interleukin-6 (IL-6) protein, a key biomarker implicated in immune responses, in the 17
- concentration range of 10 pM to 100 nM. The surface of graphene is modified with target-binding 18
- aptamers to ensure analyte selectivity. Our results show that the biosensor measurements were stable 19
- with minimum changes when the GFET was bent with a radius of curvature between 1.5 cm and 4.25 20
- cm suggesting robustness of the flexible GFET device. We have also demonstrated continuous real-21
- time monitoring of IL-6 with high sensitivity within the concentration range of 10 pM and 1nM. 22
- Furthermore, a minimum footprint, battery-powered circuit board is also developed that controls the 23
- GFET and records the sensor responses in real-time demonstrating the feasibility of becoming a fully 24
- standalone and wearable biosensor. The results from this work suggest that the thin film GFET-based 25
- biosensor has the potential to be used as a wearable continuous health monitoring device. 26

1 Introduction

27

28 One of the most effective ways to treat illnesses is early screening and diagnosis of the disease. According to the Centers for Disease Control and Prevention (CDC) in the United States, in 2018, ten 29 million people suffered from tuberculosis, a leading infectious disease in the world, however over three 30 million of those cases went undiagnosed [1]. Breast cancer is another example of life-threatening 31 disease that requires early stage testing and diagnosis for effective treatment. Early detection of breast 32 cancer has proven to allow for increased available treatment options, increased survival, and improved 33 quality of life [2]. The current COVID-19 pandemic also showcases the importance of fast, reliable, 34 and low-cost testing of the virus which could dramatically improve the survival rate of the patient when 35 36 proper treatments were administered at the early stage. Currently, most testing for disease biomarkers 37 are done at a centralized laboratory where a large number of samples are collected for testing. In order to reduce the turnaround time, from sample submission and test results, point-of-care testing (POCT) platforms have been suggested and have been recognized in the research community as a viable alternative to a lab-based testing center [3], [4].

Biosensing is an active area of research because such devices can help monitor, track, and treat a plethora of diseases, sicknesses, and conditions. Among the various biosensing platforms, graphenebased field-effect transistors (GFETs) are highly advantageous for creating simple yet reliable biosensors and thus are increasing in popularity as a biosensing platform. Graphene, a well-known semimetal with unique band structure and exceptional electronic properties [5], is ideal to be used as a transistor channel because it is extremely sensitive to charged molecules being adsorbed onto its surface resulting in a significant change in the electric field and subsequently a change in the gate potential of the device. As a result, this creates a direct change in the channel conductance which can be observed through measuring the drain-source current [6], [7]. This approach can be utilized to implement a sensor in which the drain-source current changes proportionally to the amount of the target molecule of interest and thus creating a GFET-based biosensor. Graphene-based FETs have been used in a wide variety of biosensing applications. For example, GFETs have been used to detect protein biomarkers [8]-[13], DNAs [14], and glucose [15]. Being a 2-dimensional (2-D) nanomaterial, graphene is well-suited for fabricating a thin-film transistor having a planar geometry. Moreover, the mechanical durability of a graphene film lends itself to the development of a flexible and wearable electronic device. Here, we present a wearable GFET-based detection of protein IL-6 to study the feasibility of its application as a wearable health monitoring system.

Interleukin-6 (IL-6) is a pleotropic cytokine that is produced in response to a plethora of processes including tissue damage, infections, cancer, and autoimmune diseases [16], [17]. IL-6 is also a biomarker for ailments such as collagen vascular disease, alcoholic cirrhosis, and kidney disease [18]. IL-6 is a protein which can be produced by both normal and harmful biological processes. For instance, it is produced by the body during infections and kidney disease, but it is also produced by normal cell types that are involved in processes such as reproduction, metabolism, neural development, bone remodeling, and angiogenesis [19], [20]. Interleukin-6 is an important protein to monitor as increased levels of IL-6 can require medical attention for many of the issues and illnesses mentioned above. Early detection of such conditions is key as it increases treatment options and the probability of recovery.

In this work, we demonstrate a low cost 2-D GFET fabricated on a flexible polymer film using a conductive ink printer and its use as a wearable biosensor for detecting IL-6 biomarker. Aptamers have been integrated with graphene to create target selectivity in the detection. The main contributions of this work are: (1) the demonstration of a flexible and wearable GFET-based biosensor for wearable applications; (2) the use of polyimide (Kapton) film as a bendable, robust, and thermally stable substrate for the GFET; and (3) implementation of a fully standalone miniaturized circuit board for controlling the GFET and measuring the sensor readout. We envision that such GFET-based wearable platform could potentially become a POCT device for real-time diagnosis of various health conditions.

2 Materials and Methods

2.1. Materials

79 The amine-terminated aptamer oligonucleotide with a selective affinity toward recombinant mouse interleukin-6 (IL-6) was synthesized by BasePair Biotechnologies Inc (Pearland, TX, USA). The 80 aptamers are single stranded DNAs with a length of 32 nucleotides and an average K_D of 5.4 nM [21]. 81 82 The IL-6 protein from recombinant mouse was purchased from Biolegend Inc (San Diego, CA, USA). The diluted solutions of proteins were prepared in 0.1 mM Phosphate buffer solution (PBS, pH 7.4, 83 84 Sigma-Aldrich). 1-pyrenebutyric acid N-hydroxysuccinimide ester (PBASE) was purchased from 85 Santa Cruz Biotechnology Inc (Dallas, TX, USA). The silver conductive inks were purchased from Voltera (Kitchener, ON, Canada) and Dycotec Materials Ltd (Calne, Wiltshire, UK). The CVD-grown 86 graphene film was purchased from Graphenea Inc. (San Sebastián, Spain) 87

2.2. Fabrication of GFET

88

89

90

91

92

93

94

95 96

97

98

99 100

101

102

103104

The solution-gated GFET device was fabricated by fully printing the source, drain, and the gate electrodes using a conductive ink-based PCB printer (Voltera V-One, Canada). This printer is especially ideal for plotting high viscosity inks and can print on a wide variety of substrates including polymer films. By printing the devices in-house using this hardware, it allows for rapid prototyping and low-cost fabrication of our devices. To enhance flexibility and stretchability, a commercially available stretchable silver conductive ink (Dycotec Materials, UK) was used to pattern the electrodes. The Easy Transfer monolayer graphene from Graphenea, Inc. is used to create the conductive channel between the drain and source electrodes. The graphene film contains a polymer backing and a sacrificial layer on top for passivation. To transfer the graphene film onto the flexible printed electrode, a small amount of deionized water droplet was placed on the electrode where the graphene is to be positioned using a pipette. The substrate containing the graphene film was placed on the water droplet which resulted in a separation between the graphene and the polymer backing. After removing the polymer film, the water was removed either manually using a pipette or through evaporation. Once fully dried, the GFET device was immersed in acetone, ethanol, and deionized water, sequentially (for 1 hour in each solution) to remove the sacrificial layer above the graphene. The GFET fabrication steps are outlined in Figure 1.

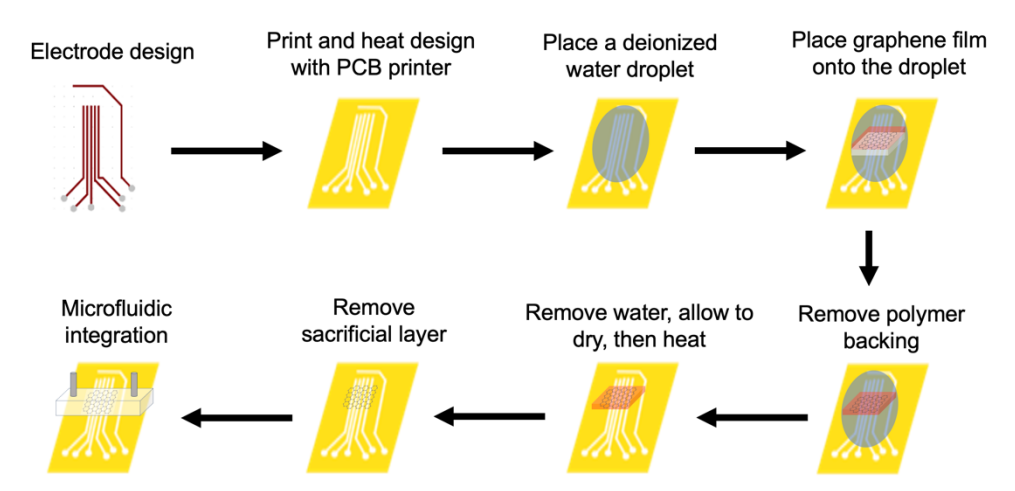


Figure 1. Overview of the fabrication process for the GFET device using KiCad software for electrode design, Voltera V-One PCB printer for electrode patterning, and using Graphenea Easy Transfer graphene film as a conductive channel of the field-effect transistor.

2.3. Aptamer Immobilization on Graphene

105

118

119

120 121

122123

124

125 126

127

128

129

130

131

132

106 The aptamer immobilization on graphene surface is achieved using PBASE as a linker. The functionalization of the solution-gated GFET device with aptamers is done by placing a 200 µL droplet 107 of 10 mM PBASE in dimethyl formamide (DMF) onto the graphene surface at room temperature for 2 108 109 hours. A silicone well (1 cm \times 0.5 cm \times 0.5 cm) was mounted on the chip across the drain and source 110 electrodes to contain the PBASE solution on the graphene surface, as DMF is highly volatile and could also interfere with the printed silver electrodes. After the PBASE incubation is complete, the substrate 111 is then washed successively with DMF, ethanol, and deionized water for 3 minutes each to remove any 112 unbound PBASE linkers on the substrate. The final step in the GFET functionalization is the 113 114 immobilization of the aptamers. Aminated (5') probe DNAs at 5 μM in 0.01× PBS mixed with 1 mM MgCl₂ are introduced to the graphene in the form of a 100 μL droplet at room temperature for two 115 hours. After incubation, the excess aptamer solution is rinsed with 0.01× PBS to remove any unreacted 116 aptamers. 117

2.4. Electrical FET measurements

All electrical measurements for both static and real-time measurements were collected using a Micromanipulator (450 PM-B) probing station in combination with a Keysight precision source/measure unit (B2902A) and National Instruments LabVIEW program. For static measurements, a constant bias voltage V_{DS} is applied across the drain and source terminals while the gate voltage V_{GS} , which is applied through the liquid gate of 0.01 X PBS buffer solution, is linearly swept typically from -2~V to +2V with a scan rate of 100 mV/s. The real-time biosensing experiments also utilize a GW Instek laboratory DC power supply, a 600 μ m by 100 μ m polydimethylsiloxane (PDMS) microfluidic channel, and a PHD Ultra syringe pump by Harvard Apparatus. For real-time measurements, both V_{DS} and V_{GS} are fixed to constant values and I_{DS} is recorded continuously while flowing the sample solutions through the microfluidic channel. Figure 2 shows the schematic diagram of the solution-gated GFET device with the electrical connections.

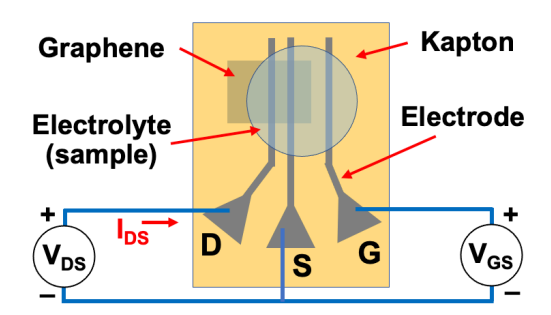


Figure 2. Schematic illustration the solution-gated GFET-based biosensor showing the electrical connections for applying V_{DS} and V_{GS} , forming a liquid gate with the electrolyte solution, and measuring the drain current I_{DS} .

3 Results and Discussion

3.1. The effects of a thin silicon dioxide coating on the FET measurements

Silicon dioxide coating has shown to enhance the sensing performances of GFET devices. Naturally occurring organic contaminants can cause poorer sensitivity in detection, decreased carrier mobility and unwanted doping of the substrate [9]. By coating a thin layer of SiO₂ on the substrate, it can not

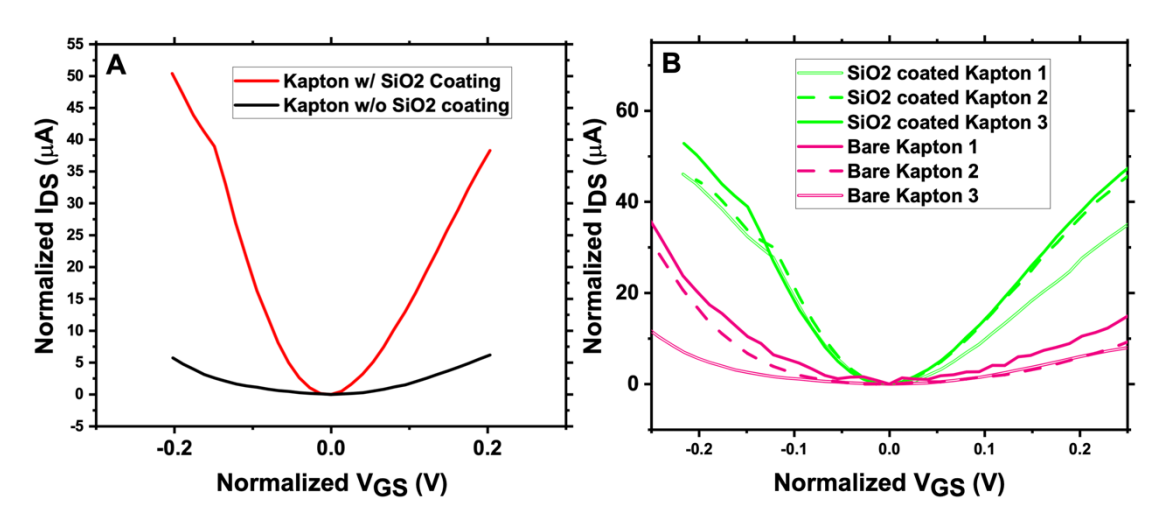


Figure 3. The transfer characteristic curves of GFET devices fabricated on (A) Kapton substrate with 50 nm SiO_2 coating versus bare Kapton film; (B) SiO_2 coating improves the consistency to the transfer characteristic curve measurements. For both plots, $V_{DS} = 100$ mV.

only offer protection for the graphene against unwanted doping but also provides a smoother surface for the substrate enabling a higher quality fabrication of the GFET device [9]. Furthermore, the coating has also been shown to significantly enhance the transconductance of the device which is directly related to the sensor sensitivity. Zhuang et al. have demonstrated that the SiO₂ coating has resulted in more consistent I-V characteristic curve for the GFET, and it also exhibited sharper edges and therefore higher transconductance near the Dirac point [9].

Prior to the electrode printing and GFET fabrication, a 50 nm SiO_2 coating was deposited onto the bare Kapton film (12 inches × 12 inches × 1 mil) using a sputter deposition system from the Nanofabrication Laboratory at the University of Massachusetts Lowell. In order to ensure the reliability of the results, the effect of a 50 nm SiO_2 coating was explored on the Kapton film. Figure 3 shows the I-V characteristic curves of the GFET fabricated on Kapton before and after SiO_2 coating. The plots are normalized such that the x-axis represent V_{GS} - V_{Dirac} , and the y-axis represent I_{DS} – I_{Dirac} . Coating the Kapton film with SiO_2 significantly increases both the transconductance of the device as well as the device consistency as demonstrated in Figure 3A and Figure 3B, respectively.

3.2. Device substrate selection

A wearable biosensor must be accommodating to the human body and thus needs to be integrated in a wearable and flexible platform. Substrate choice is key as it will ensure the safety and subsequently the effectiveness of the biosensor. Substrates such as biaxially-oriented polyethylene terephthalate (Bo PET) also known as Mylar, polyamide film named Kapton by DuPont, and polydimethylsiloxane (PDMS) are all flexible substrates that could accommodate such needs of a wearable electronics.

Kapton is a thin polyimide film which is lightweight and bendable. The Kapton film used in this work was 0.001 inches thick (~25 μm). The Kapton was able to provide structural stability and its rigidity helped prevent potential tears while still offering a bendable device. Kapton has a relatively high melting point compared to other polymers and thus can withstand extreme heat up to 400 °C [22]. Mylar is a transparent polyester film that is thin, lightweight and can conform well to the skin, thus making it a suitable substrate for a wearable device [23], [24]. It offers advantages such as a high tensile strength, electrical insulation, and stability. Disadvantages of this film include a tendency to easily crumple and tare thus causing issues for the sensor and a relatively low melting point of 250 °C.

Another disadvantage to using a Mylar film is that it frequently requires bonding to a rigid substrate during fabrication [23]. While both Mylar and Kapton are thin films that present themselves as possible candidates as a wearable device substrate, silicone materials, such as polydimethylsiloxane (PDMS) which is highly elastic and durable, can also be used as wearable substrates [25].

To select the proper substrate for the device fabrication, the KiCAD (a layout design software) design was printed onto each of the three potential substrates (Mylar, Kapton, and PDMS) which had each been coated with a 50 nm layer of SiO_2 . A silicon oxide (SiO_2) wafer substrate with the same design was also used during the process as a baseline for comparison. Graphene was then transferred across each of the four substrates and the bare graphene transfer characteristic curve of each GFET device was measured as shown in Figure 4A. The Kapton substrate exhibits the sharpest I_{DS} versus V_{GS} characteristic curve, making it the most sensitive GFET-based sensor. Mylar displays promising results as the magnitude of the current is similar to the silicon wafer which was used as a baseline. However, the GFET device fabricated on the PDMS substrate displays almost no change in current flow regardless of the gate-to-source voltage (V_{GS}) applied to the device. This excludes the PDMS substrate from being a viable option as it will make it extremely difficult to identify the Dirac voltage for a GFET with such a gradual incline. Therefore, the device is fabricated on a 50 nm SiO_2 coated Kapton substrate as shown in Figure 4D.

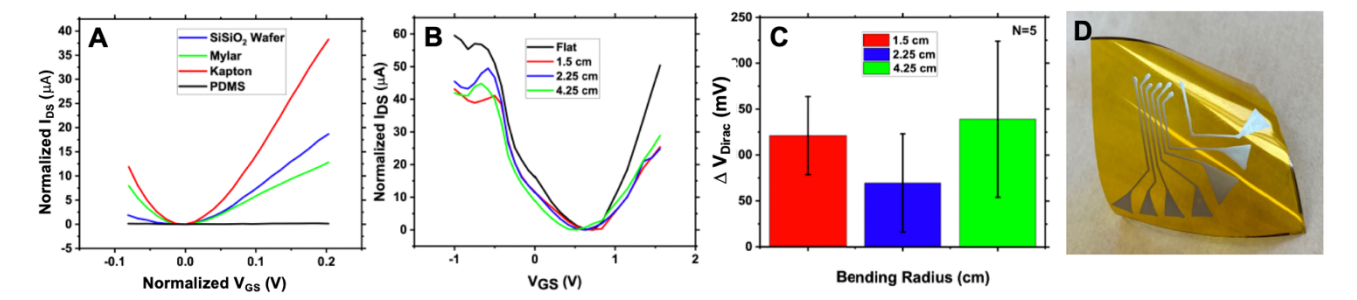


Figure 4. (A) Transfer characteristic curve with $V_{DS} = 100$ mV for Si/SiO_2 wafer (baseline), SiO_2 coated Mylar, SiO_2 coated Kapton, and SiO_2 coated PDMS. The x-axis represents $V_{GS} - V_{Dirac}$, and the y-axis represents $I_{DS} - I_{Dirac}$ so that the Dirac point is at (0,0); (B) Transfer characteristic curve of GFET on flat substrate and bent around radii of 1.5 cm, 2.25 cm, and 4.25 cm. As a reference, the flat GFET had $V_{Dirac} = 0.73$ V; (C) Change in Dirac voltage with respect to the bending radius of the substrate. Error bars are created with N = 5 devices. (D) GFET design with all parameters finalized. Substrate: 50 nm SiO_2 coated Kapton; Ink: Dycotec flexible and stretchable silver conductive ink.

3.3. Impacts of mechanical stress on FET measurements

It is essential to ensure that the flexible wearable biosensor operate reliably under various mechanical stresses, such as bending and stretching, with minimum interference from such mechanical forces. GFET-based sensors have been shown to withstand a wide range of mechanical stresses, including bending [9], [23], [26], stretching [27], twisting, and even a combination of these stresses [23]. In order to understand the appropriate range of substrate bending that the GFET can withstand, the Kapton substrate was characterized under different bending radii. To test the sensor response under various bending conditions, the GFET device was bent using three different inward bending substrates (with GFET on the inside when rolled up) with the radii of 4.25 cm, 2.25 cm, and 1.5 cm. Then, the GFET I-V characteristic curves were compared against those under an unbent (device on a flat surface) condition. The inward bending of the device was chosen to mimic a scenario where the GFET is facing the skin for applications such as sweat-based bioanalytical sensors. As can be seen in Figure 4B, the

inward bending of the substrate did cause some variations in the transfer characteristic curve presumably due to the change in carrier mobility caused by the mechanical deformation of the graphene film. Figure 4C shows the change in Dirac voltage compared to the unbent device for each bending radius of the substrate. Such shifting in the Dirac voltage with respect to bending radius is consistent with previous works [9]. However, the mechanical stress imposed on a bent GFET and, consequently, its effect on the I-V characteristics are relatively mild (compared to stretching of graphene which would significantly impact the electronic properties of the GFET), and therefore, the device is able to withstand a moderate degree to bending on the substrate. Unlike, substrate bending does not impose a significant mechanical stress on graphene Moreover, it can be expected that further miniaturization of the GFET design will make the sensor more robust and less susceptible to mechanical deformations. The results obtained from these analyses suggest that the biosensor can operate properly in all of the bending conditions studied in this work.

3.4. The effects of graphene functionalization and target specificity of the GFET device

193

194

195

196

197

198

199

200

201202

203204

205

206

207208

209

210211

212

213

214

215

216217

218

219

220

221

222

The immobilization of aptamers onto the graphene surface is critical for eliciting target-specific biosensing responses from the solution-gated GFET. Figure 5A and Figure 5B show the current response of the bare GFET to IL-6 exposure in the absence of the aptamers. Without the aptamers present on the graphene surface, there is a negligible shift in the Dirac voltage for the bare graphene under various concentrations of IL-6 that were introduced as shown in Figure 5A. Figure 5B displays the change in Dirac voltage as a function of the analyte concentration which is minimal and concentration independent. This indicates that without the incorporation of the linkers and targetbinding aptamers, the target proteins are not able to effectively influence the graphene conducting channel. Figure 5C shows the effects of graphene surface modification on the I-V characteristics. The immobilization of the PBASE linker onto the graphene surface causes a p-type doping effect resulting in a right-shift of the transfer characteristic curve and the Dirac voltage [28], [29]. The carbonyl group of PBASE is an electron-withdrawing group and therefore causes an electron transfer to occur from the graphene to the linker, creating a positive shift in the Dirac voltage [30]. Further modification of graphene by crosslinking aptamers to PBASE causes a left-shift in the I-V characteristics, compared to the PBASE-modified graphene, because of the n-type doping due to the negatively charged DNA strands serving as electron donors when they interact with the graphene surface [30]. Such shifting of the I-V curves is consistent with previously reported results [9], [12], [30].

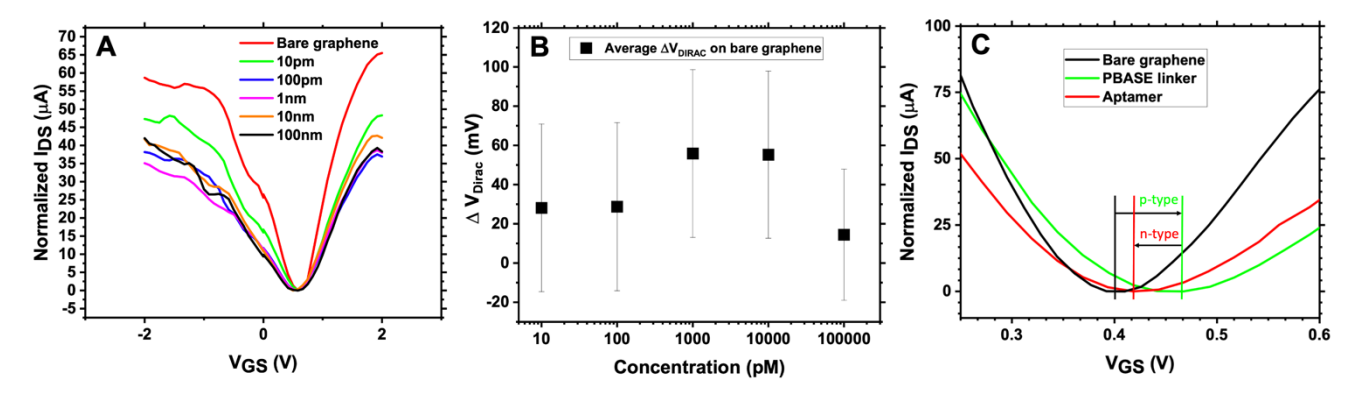


Figure 5. IL-6 sensing performed on a Kapton-based GFET device without PBASE and aptamers attached: (A) GFET transfer characteristic curves with $V_{DS} = 50$ mV; (B) The corresponding calibration curve. The error bars are generated with N = 6 devices and represent one standard error; (C) Transfer characteristic curves during functionalization displaying p-type doping after introduction of PBASE and n-type doping after introduction of aptamers.

3.5. Static mode for IL-6 detection: gate voltage sweep

The static mode of IL-6 detection is performed by linearly sweeping the gate-source voltage (V_{GS}) while maintaining a fixed drain-source voltage (V_{DS}) and measuring the drain current (I_{DS}). In this sensing mode, the concentration of the target analyte is predicted by observing a shift in the Dirac point. Here, we have taken two different approaches to the static mode sensing: (1) buffer liquid gating and (2) analyte liquid gating. The differences between the two approaches are outlined in Figure 6. In the buffer liquid gating approach, the target analyte is exposed to the sensor for 10 minutes, followed by rinsing and placing a buffer solution of $0.01 \times PBS$ for the I-V measurements. The results from the static buffer liquid-gated method are displayed in Figure 6B and Figure 6C which show the corresponding transfer characteristic curves and the change in Dirac voltage as a function of IL-6 concentration, respectively. In the analyte liquid gating approach, there is no rinsing step, but instead the analyte containing buffer is directly used as the liquid gate during the I-V measurements. The results from the static analyte liquid-gated method are displayed in Figure 6D and Figure 6E showing the resulting transfer characteristic curves and the change in Dirac voltage as a function of IL-6 concentration, respectively. While the buffer liquid gating method is desirable as it eliminates the chances of non-specifically bound targets impacting the sensing measurements, the analyte liquid

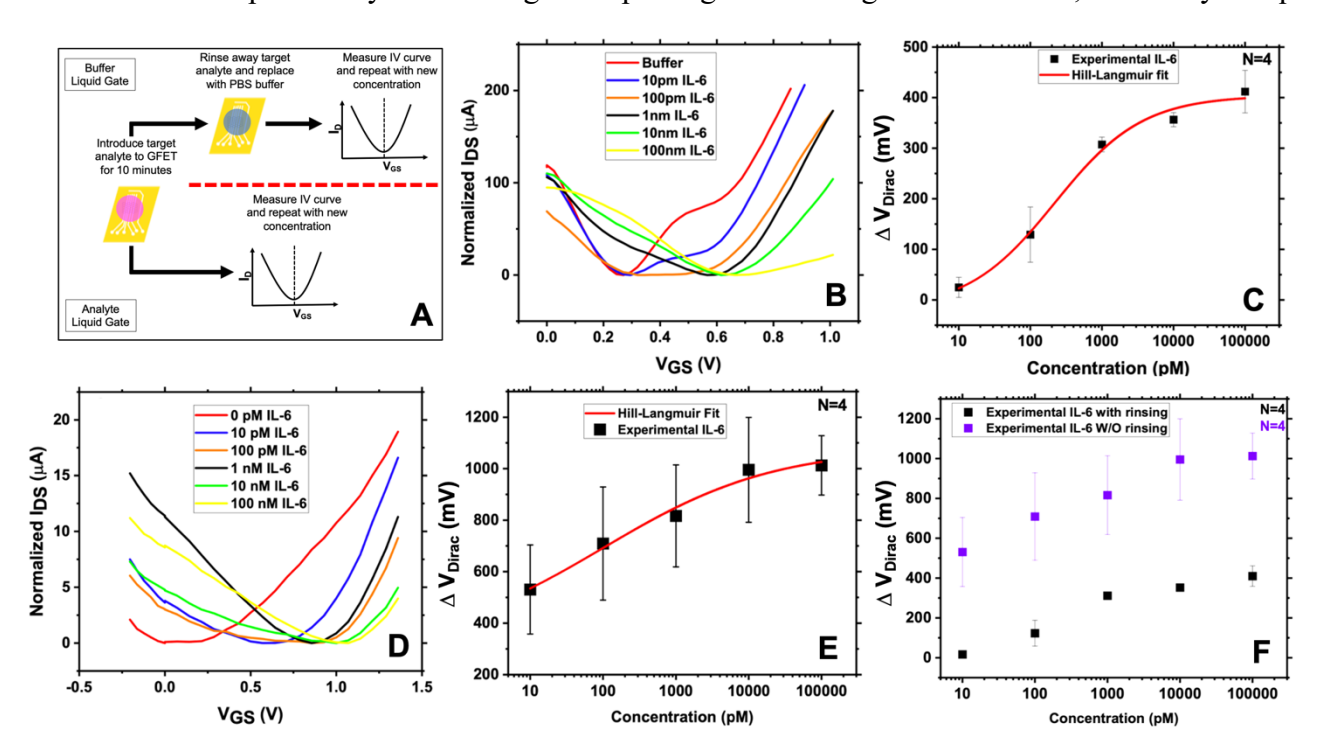


Figure 6. (A) Illustration of the buffer liquid-gated (device rinsed after sample exposure) versus analyte liquid-gated (no rinsing after sample exposure) sensing approaches; (B) The transfer characteristic curves for the buffer liquid-gated IL-6 static sensing with $0.01 \times PBS$ as a liquid gate and $V_{DS} = 100$ mV; (C) The buffer liquid-gated IL-6 sensing calibration curve with the Hill-Langmuir line of best fit ($R^2 = 99.27\%$, N = 4); (D) The transfer characteristic curves for the analyte liquid-gated IL-6 static sensing with IL-6 added into $0.01 \times PBS$ as liquid gate and $V_{DS} = 10$ mV; (E) Analyte liquid-gated IL-6 sensing calibration curve with the Hill-Langmuir line of best fit ($R^2 = 98.37\%$, N = 4). (F) comparison of the IL-6 calibration curves between rinsing (buffer liquid gate) and non-rinsing (analyte liquid gate) methods.

gating method reduces the chances of the receptor-bound targets from dissociating from the aptamers by eliminating the device rinsing step. As shown in Figure 6F, there is a greater shift in the Dirac voltage for the non-rinsed method (analyte liquid-gated) compared to the devices that were rinsed after analyte exposure (buffer liquid-gated). However, the buffer liquid-gated sensors exhibited higher reproducibility as indicated by the error bars in the data points.

A wearable device needs to be able to withstand material deformations while its performance integrity stays intact. Other Mylar-based biosensors have proven to be able to withstand deformations such as substrate bending [9], [15], twisting, and stretching [23]. It is vital that the wearable sensor measurement be minimally impacted by such deformations in the device. In order to characterize the sensing performances of the developed biosensor under mechanical stress, the fabricated GFET-based IL-6 sensor was bent (with device facing outward) with a radius of 2.25 cm and the static sensing process was repeated as shown in Figure 7. A known concentration of IL-6 in 0.01× PBS was used as the liquid gate with a V_{DS} of 10 mV. Figures 7A and 7B show that even under the bending condition, the device still exhibits distinct transfer characteristic curves and the concentration dependent right-shift of the Dirac voltage indicating the robustness and the stability of the Kapton-based GFET device. Finally, Figure 7C shows the comparison between sensing on flat and bent substrates. The bending of the substrate results in a reduced shift in the Dirac point compared to the flat substrate possibly due to the disruption in the graphene lattice structure which may negatively impact the mobility of the carriers.

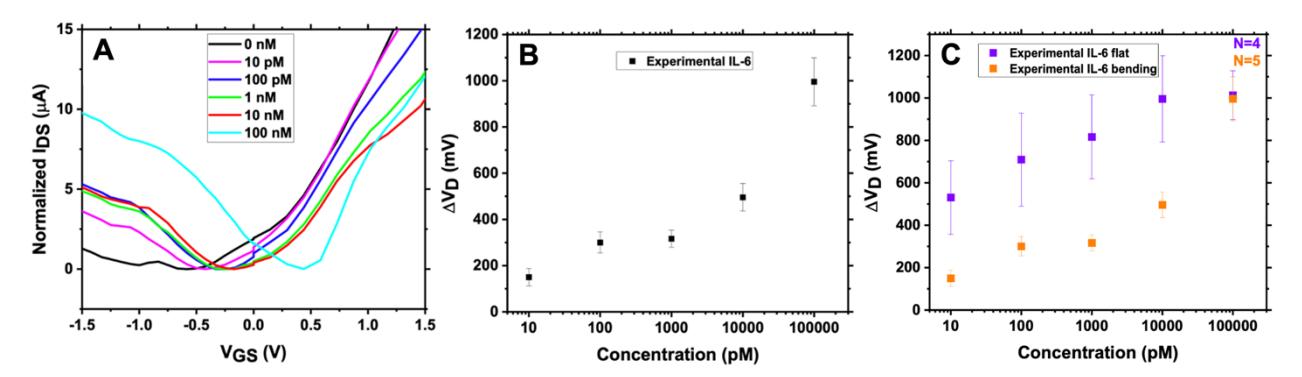


Figure 7. (A) Kapton-GFET IL-6 static sensing results while substrate is bent at radius of 2.25 cm and $V_{DS} = 10$ mV; (B) Concentration calibration curve showing change in Dirac voltage as a function of concentration. (C) Comparison of calibration curves with IL-6 sensing done with GFET on flat substrate (purple) and on bent substrate (orange). The error bars represent one standard error with N = 5.

To provide perspective and comparison of this work with other similar work in the literature, Table 1 summarizes some of the recent publications on GFET-based biosensors. Our Kapton-based GFET resulted in the detection limit of 10 pM and the detection range of $10 \, \mathrm{pM} - 100 \, \mathrm{nM}$ which is comparable to other published work in the literature. Furthermore, whereas most work on GFET-based biosensors report on point-of-care and portable devices for screening biomarkers, this work focuses on bendable and flexible GFET devices and provides new insight into the wearability of the GFET-based electronics and biosensors.

Table 1. Summary of recently published work on GFET-based biosensors.

Analyte	Detection Range	Limit of Detection	Flexible/ Wearable	Reference
Exosome	$0.1 - 10 \ \mu g/mL$	0.1 μg/mL	No	[31]
Acetylcholine	$5 - 1,000 \mu M$	2.3 μΜ	No	[32]
Biotin	0.37 pM - 16.28 nM	0.37 pM	No	[33]
SARS-CoV-2	1 fg/mL - 10 pg/mL	16 fg/mL	No	[34]
Insulin	$100 \text{ pM} - 1 \mu\text{M}$	35 pM	No	[28]
TNF-α	50 pM – 500 nM	26 pM	Yes	[9]
IL-6	1.5 pM – 100 nM	139 fM	No	[12]
IL-6	10 pM – 100 nM	10 pM	Yes	This work

3.5. Dynamic mode for IL-6 detection: real-time continuous monitoring of IL-6

One of the main advantages of GFET as a biosensing platform is its label-free and continuous detection capability. Furthermore, if implemented as a wearable sensor, it will be crucial to have the ability to monitor biomarkers in real-time, especially in the context of personalized medicine, point-of-care, and the internet of medical things (IoMT). For the dynamic mode (or continuous real-time monitoring) of IL-6 detection, both the gate-to-source voltage (V_{GS}) as well as the drain-to-source voltage (V_{DS}) is fixed to a constant value, and the sensor response is monitored by reading the changes in the drain-tosource current (I_{DS}) over time. For sequentially introducing the fluid with different IL-6 concentrations, a PDMS-based microfluidic channel was mounted over a GFET substrate to implement a lateral flow mechanism. As shown in Figure 8, when IL-6 is introduced to the device (injection time indicated by vertical dotted lines in Figure 8A), the drain current decreases in response. Since the IL-6 binding to the aptamers causes a right-shift in the I-V curves, with the GFET biased to the right side of the Dirac point ($V_{GS} = 1.3 \text{ V}$), a drop in I_{DS} as a function of increasing IL-6 concentration is consistent with the measurements obtained in the static sensing mode. For each concentration, it can be observed that I_{DS} initially stabilizes but gradually drifts as time progresses. This is expected as the graphene surface condition may be changing as more analytes interact with the surface of graphene. Figure 8B displays the average change in drain-to-source current for the real-time IL-6 detection.

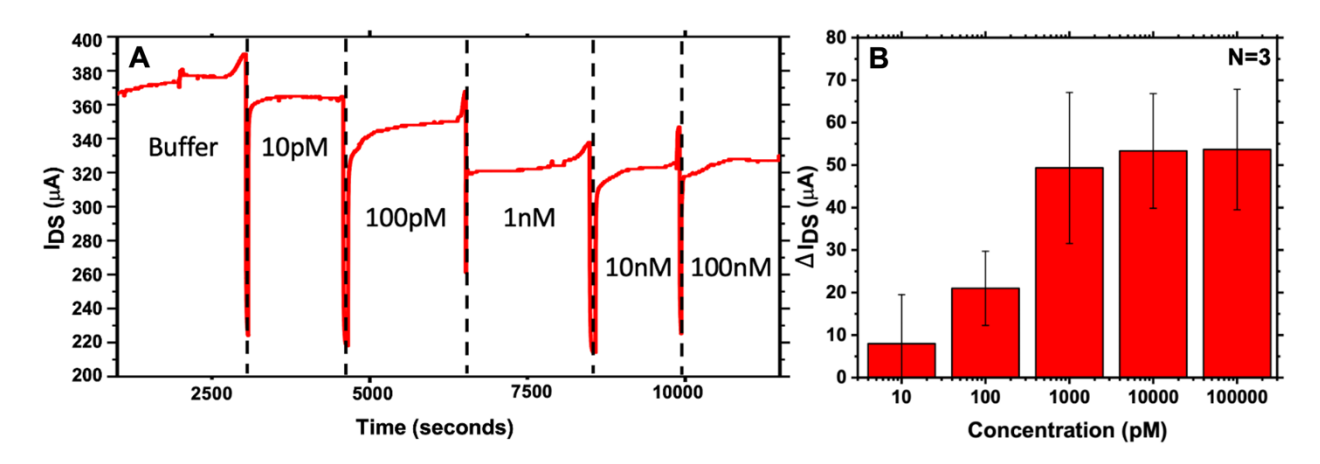


Figure 8. Continuous real-time monitoring of the IL-6 biomarker: (A) I_{DS} vs. time with various concentrations of IL-6. Sample injection time is indicated with vertical dotted lines; (B) Change in I_{DS} with respect to IL-6 concentration (N = 3). The GFET voltage parameters were $V_{GS} = 1.3$ V and $V_{DS} = 100$ mV. The microfluidic flowrate was 20 μ L/min.

4 Implementing the wearable electronics

296

297

298

299

300

301

302

303

304 305

306

307

308 309

310 311

312

313

314

315

For implementing a fully standalone and wearable biosensing device, the bulky instruments used for operating the GFET, namely the source measure unit, power supply, micromanipulator, and a computer with the LabVIEW software, were removed and replaced with a miniaturized and portable circuit board containing a coin cell battery, a voltage control system, a current meter, and the data acquisition and storage system as shown in Figure 9A. One of the major challenges when measuring a low current in the micro to nano ampere range with a low voltage current meter is the burden voltage. Burden voltage is the voltage drop across a shunt resistor through which a current to be measured passes. This can result in significant loss of resolution and accuracy. To address this issue, a custom-made analog front end (AFE) device with an ultra-low offset (<50 µV) and a low noise precision amplifier (< -90 dBV) was developed by Dr. Mahmud's group. The AFE is operated with zero bias voltage to continually correct for the DC offset voltage of the main amplifier. Afterward, the signal is fed into a 24-bit analog to digital converter with digital filtering. The output data rate is programmable, with the slowest speed (4.17 Hz) giving the lowest noise of 40 nV, which is negligible compared to other sources of noise. The device is operated by simply recording the drain-to-source current (I_{DS}) overtime and taking samples every 500 msec. This portable measuring system records the data and instantly sends it to a laptop computer via a USB cable. The first implementation of the wearable device was created on a rigid PCB substrate. The initial measurements are done to ensure integration is possible and that the device works as anticipated when paired with the GFET biosensor.

When implementing an integrated current measurement platform to the Kapton-based GFET device, it is vital that the data measured in this integrated platform closely match that obtained by the Keysight source measure unit for validation. To ensure that the portable integrated device is providing accurate data, the I_{DS} measurements of a GFET device were taken simultaneously using both the integrated platform and the conventional system using Keysight source measure unit and the LabVIEW software. Three individual GFET devices were prepared and each GFET measurement was repeated three times to characterize both the device-to-device reproducibility as well as the single device reproducibility. As can be seen in Figure 9B, the current measured by the portable platform matches closely to that of the Keysight instruments. A slight right-shift of about 100 mV in the I-V curve obtained by the integrated microcontroller, when compared against that for the conventional system, can be attributed to the presence of a digital filter based on a rolling average calculation over multiple data points. As shown in Figure 9C, this small shift in the Dirac voltage between the portable device and the conventional measurement is consistent among the three devices. Designing a higher performing filter or manually offsetting this shift may further improve the accuracy of the portable current measurement device and may even more closely match the I-V curve of the traditional instrumentation. It should also be noted that the integrated microcontroller device does exhibit a slightly higher noise and variation in the measurement compared to the conventional setup as expected.

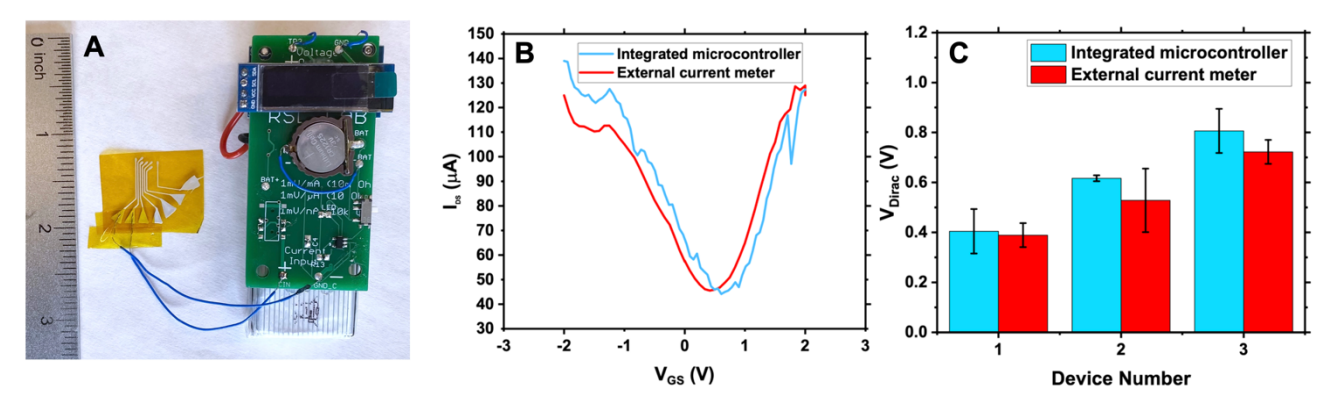


Figure 9. (A) The Kapton-GFET sensor shown with the integrated miniaturized circuit for GFET control and measurement; (B) Comparison between the I_{DS} vs. V_{GS} transfer characteristic curves measured by the integrated microcontroller (portable device) and the external source measure unit (Keysight B2902A); (C) the positions of the Dirac voltage measured with two different systems (N = 3 per device).

5 Conclusion

316

317318

319

320 321

322

323

324325

326

327328

329

330331

332

333

334

335

336

337

338

339340

341

342343

344345

In this work, we have presented a fully printable, graphene-based FET biosensor for the sensitive static and dynamic (real-time) aptameric sensing of Interleukin-6 (IL-6) protein biomarker. The biosensor is fabricated with a 2D PCB printer and a silver conductive ink, using a KiCAD for electrode design. The GFET is fabricated onto a 50 nm SiO₂ coated Kapton film. We have demonstrated static sensing using both the buffer liquid gating method as well as the analyte liquid gating method where both cases display a rightward concentration dependent shift in the Dirac point. While buffer liquid gating shows a more reproducible results, the analyte liquid gating resulted in a greater shift in the Dirac point leading to higher sensitivity. The device is also shown to be capable of continuous real-time sensing as there is a clear change in the drain-source current upon introduction of a sample fluid with different IL-6 concentrations. The developed GFET biosensor is able to detect IL-6 concentrations ranging from 10 pM to 100 nM. Finally, we have also demonstrated the potential for our sensing platform to be used as

- a truly standalone and wearable device by developing a portable and miniaturized electronic unit that
- can operate the GFET biosensor. For future improvements, developing an integrated microcontroller
- unit on a flexible PCB film and adding a wireless data transfer module would make this platform highly
- convenient and practical for wearable biosensing applications.

350 **6** Conflict of Interest

- 351 The authors declare that the research was conducted in the absence of any commercial or financial
- relationships that could be construed as a potential conflict of interest.

353 7 Author Contributions

- E.S., and M.S.M. conceived the concept of the printable and wearable electronic platform. K.L., N.K.,
- and E.S. developed the Kapton-GFET-based device for the biosensing of IL-6; K.L. performed the
- device fabrication, characterization, and collected the experimental data; K.L., E.S., and M.S.M. wrote
- 357 the manuscript; M.S.M. and P.S. developed the portable integrated microcontroller unit and assisted in
- data collection with the device. K.L., N.K., and E.S. performed data analysis; E.S. oversaw the project
- and performed the overall editing of the manuscript.

360 8 Funding

- This project was funded in part by the National Science Foundation (ECCS, Grant #: 1847152) and
- the NSF EPSCoR (Grant #: 1757371) and the UNH College of Engineering and Physical Sciences
- 363 (CEPS) Graduate Assistantship (K.L.).

364 9 Acknowledgments

- The authors would like to thank Thomas Ferraguto from the Nanofabrication Laboratory at the
- 366 University of Massachusetts Lowell for his assistance in coating silicon dioxide on all the substrates
- used in this work.

368 10 References

- "Global Health Newsroom Tuberculosis." Centers for Disease Control and Prevention, Apr.
 06, 2020. [Online]. Available: www.cdc.gov/globalhealth/newsroom/topics/tb/index.html
- 371 [2] "Early Detection of Breast Cancer Information." Oct. 31, 2018. [Online]. Available:
- 372 www.myvmc.com/investigations/early-detection-of-breast-cancer/
- 373 [3] A. St John and C. P. Price, "Existing and Emerging Technologies for Point-of-Care Testing," *Clin. Biochem. Rev.*, vol. 35, no. 3, pp. 155–167, Aug. 2014.
- Y.-C. Syu, W.-E. Hsu, and C.-T. Lin, "Review—Field-Effect Transistor Biosensing: Devices and Clinical Applications," *ECS J. Solid State Sci. Technol.*, vol. 7, no. 7, pp. Q3196–Q3207,
- 377 2018, doi: 10.1149/2.0291807jss.
- 378 [5] G. Lu, K. Yu, Z. Wen, and J. Chen, "Semiconducting graphene: converting graphene from semimetal to semiconductor," *Nanoscale*, vol. 5, no. 4, p. 1353, 2013, doi: 10.1039/c2nr32453a.
- 380 [6] J. Park, H. H. Nguyen, A. Woubit, and M. Kim, "Applications of Field-Effect Transistor (FET)-
- Type Biosensors," Appl. Sci. Converg. Technol., vol. 23, no. 2, pp. 61–71, Mar. 2014, doi:
- 382 10.5757/ASCT.2014.23.2.61.

- N. I. Khan, "Nanoelectronic Devices for Sensitive Detection of Biomarkers in Healthcare Monitoring," University of New Hampshire, 2021.
- [8] S. Ghosh, N. I. Khan, J. G. Tsavalas, and E. Song, "Selective Detection of Lysozyme Biomarker
 Utilizing Large Area Chemical Vapor Deposition-Grown Graphene-Based Field-Effect
 Transistor," *Front. Bioeng. Biotechnol.*, vol. 6, p. 29, Mar. 2018, doi:
 10.3389/fbioe.2018.00029.
- Z. Hao *et al.*, "Measurement of cytokine biomarkers using an aptamer-based affinity graphene nanosensor on a flexible substrate toward wearable applications," *Nanoscale*, vol. 10, no. 46, pp. 21681–21688, 2018, doi: 10.1039/C8NR04315A.
- [10] M. Bandyopadhyay, G. Chakraborty, S. Roy, and S. Bhattacharjee, "Study of Graphene field effect transistor (GFET) for chemical sensing application.," *J. Phys. Conf. Ser.*, vol. 1797, no. 1, p. 012045, Feb. 2021, doi: 10.1088/1742-6596/1797/1/012045.
- [11] Z. Hao, Y. Pan, W. Shao, Q. Lin, and X. Zhao, "Graphene-based fully integrated portable nanosensing system for on-line detection of cytokine biomarkers in saliva," *Biosens. Bioelectron.*, vol. 134, pp. 16–23, Jun. 2019, doi: 10.1016/j.bios.2019.03.053.
- Z. Hao, Y. Pan, C. Huang, Z. Wang, and X. Zhao, "Sensitive detection of lung cancer
 biomarkers using an aptameric graphene-based nanosensor with enhanced stability," *Biomed. Microdevices*, vol. 21, no. 3, p. 65, Sep. 2019, doi: 10.1007/s10544-019-0409-6.
- 401 [13] C. Reiner-Rozman, M. Larisika, C. Nowak, and W. Knoll, "Graphene-based liquid-gated field 402 effect transistor for biosensing: Theory and experiments," *Biosens. Bioelectron.*, vol. 70, pp. 403 21–27, Aug. 2015, doi: 10.1016/j.bios.2015.03.013.
- 404 [14] B. Cai, S. Wang, L. Huang, Y. Ning, Z. Zhang, and G.-J. Zhang, "Ultrasensitive Label-Free 405 Detection of PNA–DNA Hybridization by Reduced Graphene Oxide Field-Effect Transistor 406 Biosensor," *ACS Nano*, vol. 8, no. 3, pp. 2632–2638, Mar. 2014, doi: 10.1021/nn4063424.
- 407 [15] C. Huang, Z. Hao, T. Qi, Y. Pan, and X. Zhao, "An integrated flexible and reusable graphene field effect transistor nanosensor for monitoring glucose," *J. Materiomics*, vol. 6, no. 2, pp. 308–314, Jun. 2020, doi: 10.1016/j.jmat.2020.02.002.
- 410 [16] N. Vainer, C. Dehlendorff, and J. S. Johansen, "Systematic literature review of IL-6 as a biomarker or treatment target in patients with gastric, bile duct, pancreatic and colorectal cancer," *Oncotarget*, vol. 9, no. 51, pp. 29820–29841, Jul. 2018, doi: 10.18632/oncotarget.25661.
- [17] L. Velazquez-Salinas, A. Verdugo-Rodriguez, L. L. Rodriguez, and M. V. Borca, "The Role of
 Interleukin 6 During Viral Infections," *Front. Microbiol.*, vol. 10, p. 1057, May 2019, doi:
 10.3389/fmicb.2019.01057.
- [18] F. F. Kreiner, J. M. Kraaijenhof, M. von Herrath, G. K. K. Hovingh, and B. J. von Scholten, "Interleukin 6 in diabetes, chronic kidney disease, and cardiovascular disease: mechanisms and therapeutic perspectives," *Expert Rev. Clin. Immunol.*, vol. 18, no. 4, pp. 377–389, Apr. 2022, doi: 10.1080/1744666X.2022.2045952.
- 421 [19] Y. Guo, F. Xu, T. Lu, Z. Duan, and Z. Zhang, "Interleukin-6 signaling pathway in targeted therapy for cancer," *Cancer Treat. Rev.*, vol. 38, no. 7, pp. 904–910, Nov. 2012, doi: 10.1016/j.ctrv.2012.04.007.

- [20] B. E. Lippitz and R. A. Harris, "Cytokine patterns in cancer patients: A review of the correlation between interleukin 6 and prognosis," *OncoImmunology*, vol. 5, no. 5, p. e1093722, May 2016, doi: 10.1080/2162402X.2015.1093722.
- 427 [21] "IL-6 Aptamer Data Sheet." BasePair Biotechnologies, Inc., May 18, 2021. [Online]. Available: https://www.basepairbio.com/wp-content/uploads/2017/04/ATW0082-Mouse-IL-6-429 Aptamer 7May18.pdf
- 430 [22] "DuPontTM Kapton® Polyimide Films." Dupont Electronic Solutions, 2021. [Online]. 431 Available: www.dupont.com/electronic-materials/kapton-polyimide-film.html
- [23] Z. Wang *et al.*, "An Ultraflexible and Stretchable Aptameric Graphene Nanosensor for
 Biomarker Detection and Monitoring," *Adv. Funct. Mater.*, vol. 29, no. 44, p. 1905202, Nov.
 2019, doi: 10.1002/adfm.201905202.
- [24] Z. Wang, Z. Hao, S. Yu, C. Huang, Y. Pan, and X. Zhao, "A Wearable and Deformable
 Graphene-Based Affinity Nanosensor for Monitoring of Cytokines in Biofluids,"
 Nanomaterials, vol. 10, no. 8, p. 1503, Jul. 2020, doi: 10.3390/nano10081503.
- 438 [25] S. Bhansali and A. Vasudev, MEMS for Biomedical Applications, 1st ed. Woodhead Publishing.
- 439 [26] Y. Liang, X. Liang, Z. Zhang, W. Li, X. Huo, and L. Peng, "High mobility flexible graphene 440 field-effect transistors and ambipolar radio-frequency circuits," *Nanoscale*, vol. 7, no. 25, pp. 441 10954–10962, 2015, doi: 10.1039/C5NR02292D.
- 442 [27] C. Yan, J. H. Cho, and J.-H. Ahn, "Graphene-based flexible and stretchable thin film transistors," *Nanoscale*, vol. 4, no. 16, p. 4870, 2012, doi: 10.1039/c2nr30994g.
- 444 [28] Z. Hao *et al.*, "Real-Time Monitoring of Insulin Using a Graphene Field-Effect Transistor 445 Aptameric Nanosensor," *ACS Appl. Mater. Interfaces*, vol. 9, no. 33, pp. 27504–27511, Aug. 446 2017, doi: 10.1021/acsami.7b07684.
- 447 [29] S. Xu *et al.*, "Real-time reliable determination of binding kinetics of DNA hybridization using a multi-channel graphene biosensor," *Nat. Commun.*, vol. 8, no. 1, p. 14902, Apr. 2017, doi: 10.1038/ncomms14902.
- 450 [30] X. Wang, Z. Hao, T. R. Olsen, W. Zhang, and Q. Lin, "Measurements of aptamer–protein 451 binding kinetics using graphene field-effect transistors," *Nanoscale*, vol. 11, no. 26, pp. 12573– 452 12581, 2019, doi: 10.1039/C9NR02797A.
- 453 [31] D. Kwong Hong Tsang *et al.*, "Chemically Functionalised Graphene FET Biosensor for the Label-free Sensing of Exosomes," *Sci. Rep.*, vol. 9, no. 1, p. 13946, Dec. 2019, doi: 10.1038/s41598-019-50412-9.
- [32] G. E. Fenoy, W. A. Marmisollé, O. Azzaroni, and W. Knoll, "Acetylcholine biosensor based on the electrochemical functionalization of graphene field-effect transistors," *Biosens. Bioelectron.*, vol. 148, p. 111796, Jan. 2020, doi: 10.1016/j.bios.2019.111796.
- 459 [33] S. Wang *et al.*, "Graphene field-effect transistor biosensor for detection of biotin with ultrahigh 460 sensitivity and specificity," *Biosens. Bioelectron.*, vol. 165, p. 112363, Oct. 2020, doi: 461 10.1016/j.bios.2020.112363.
- [34] G. Seo *et al.*, "Rapid Detection of COVID-19 Causative Virus (SARS-CoV-2) in Human
 Nasopharyngeal Swab Specimens Using Field-Effect Transistor-Based Biosensor," *ACS Nano*,
 vol. 14, no. 4, pp. 5135–5142, Apr. 2020, doi: 10.1021/acsnano.0c02823.

465